OPEN ACCESS
Marine Sciences ARTICLE

Multi-year La Niña dampens the Southern Oscillation during subsequent El Niño through tropical Pacific-rooted dynamics

Hanjie Fan,[1,2] Shuheng Lin,[3] Lei Zhang,[4,5] Kaiqiang Deng,[1,2] Haolin Luo,[6] Mingmei Xie,[7] Teng Wang,[8] Song Yang,[1,2,*] and Chunzai Wang[4,5,*]

*Correspondence: yangsong3@mail.sysu.edu.cn (S.Y.); cwang@scsio.ac.cn (C.W.)

Received: October 10, 2025; Accepted: April 13, 2026; Published Online: April 20, 2026; https://doi.org/10.59717/j.xinn-geo.2026.100224

GRAPHICAL ABSTRACT

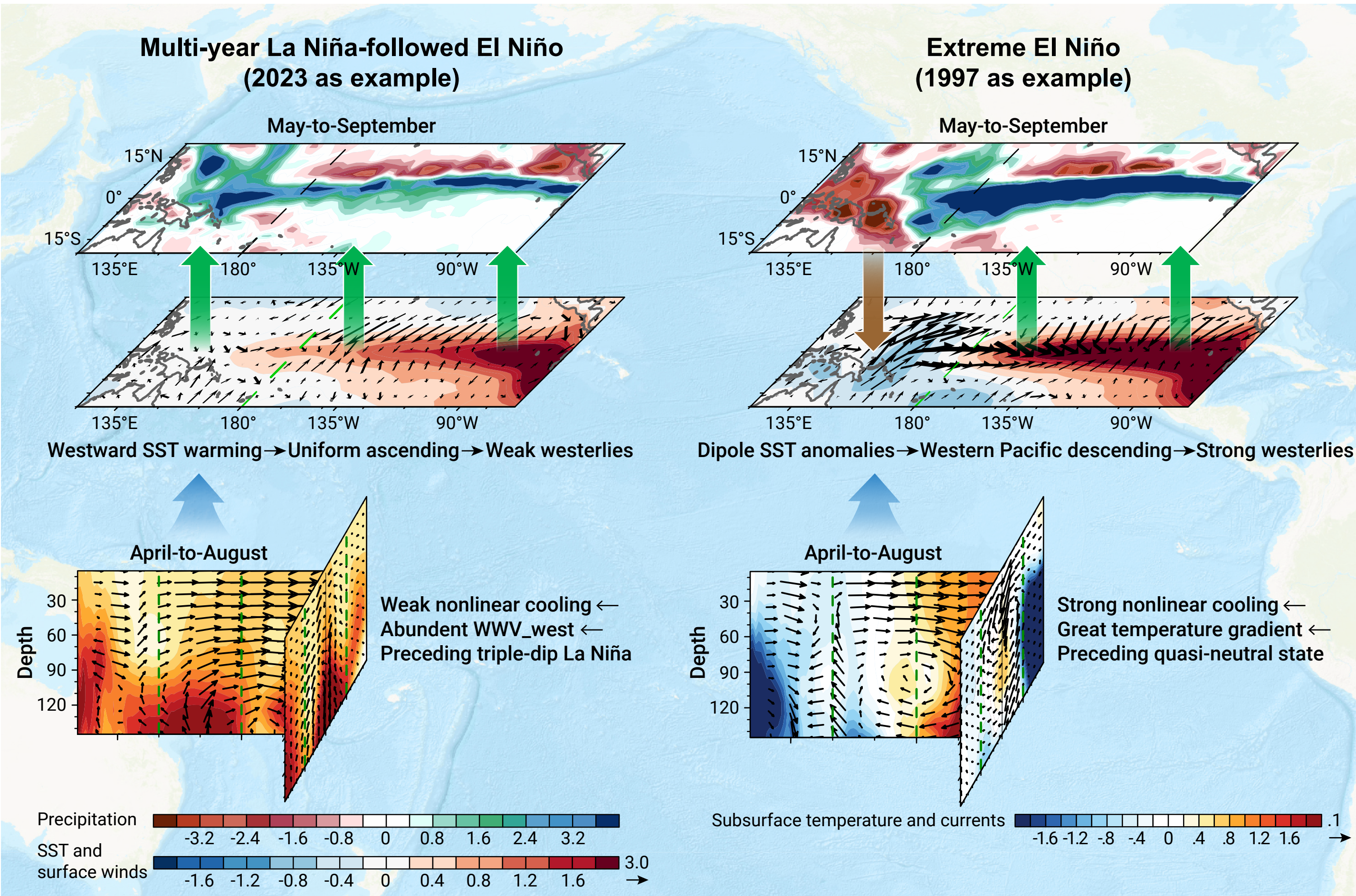

PUBLIC SUMMARY

- The 2023 strong El Niño event was unexpectedly accompanied by weak Southern Oscillation (westerly anomaly).
- This phenomenon was caused by zonally uniform ascent from westward-extended equatorial SST warming.
- The preceding multi-year La Niña (ML) accumulated abundant warm water in the western Pacific (WP).
- This warm water suppressed the nonlinear dynamical cooling in the WP during 1997-like extreme El Niños.
- This mechanism, rooted in tropical Pacific, also functioned in other El Niños after ML, especially 2009.

Multi-year La Niña dampens the Southern Oscillation during subsequent El Niño through tropical Pacific-rooted dynamics

Hanjie Fan,[1,2] Shuheng Lin,[3] Lei Zhang,[4,5] Kaiqiang Deng,[1,2] Haolin Luo,[6] Mingmei Xie,[7] Teng Wang,[8] Song Yang,[1,2,*] and Chunzai Wang[4,5,*]

[1]School of Atmospheric Sciences, Sun Yat-sen University; Southern Marine Science and Engineering Guangdong Laboratory (Zhuhai), Zhuhai 519000, China

[2]Guangdong Province Key Laboratory for Climate Change and Natural Disaster Studies, Sun Yat-sen University, Zhuhai 519000, China

[3]Key Laboratory of Humid Subtropical Eco-geographical Process (Ministry of Education), College of Geographical Sciences, Fujian Normal University, Fuzhou 350007, China

[4]Laboratory of Tropical Oceanography, South China Sea Institute of Oceanology, Chinese Academy of Sciences, Guangzhou 510000, China

[5]Global Ocean and Climate Research Center, South China Sea Institute of Oceanology, Chinese Academy of Sciences, Guangzhou 510000, China

[6]Department of Atmospheric Sciences, Climate Change and Resource Utilization in Complex Terrain Regions Key Laboratory of Sichuan Province, Chengdu University of Information Technology, Chengdu 610000, China

[7]Frontier Science Center for Deep Ocean Multispheres and Earth System, and Physical Oceanography Laboratory, Ocean University of China, Qingdao 266000, China

[8]College of Aviation Meteorology, Civil Aviation Flight University of China, Chengdu 610000, China

*Correspondence: yangsong3@mail.sysu.edu.cn (S.Y.); cwang@scsio.ac.cn (C.W.)

Received: October 10, 2025; Accepted: April 13, 2026; Published Online: April 20, 2026; https://doi.org/10.59717/j.xinn-geo.2026.100224

Citation: Fan H., Lin S., Zhang L., et al. (2026). Multi-year La Niña dampens the Southern Oscillation during subsequent El Niño through tropical Pacific-rooted dynamics. *The Innovation Geoscience* **4**:100224.

The 2023 El Niño, which occurred after a triple-dip La Niña, displayed several distinct features. Although the favorable warm water volume pre-condition indicated the potential for an extreme event, its actual intensity did not meet expectations. More counterintuitively, the westerly wind anomalies were much weaker relative to the sea surface temperature (SST) warming, presenting an unusual "strong El Niño but weak Southern Oscillation" characteristic. Here we propose a tropical Pacific-rooted mechanism that the relatively westward extension of SST warming in the equatorial Pacific was the primary cause of the weak westerly anomalies by suppressing the negative convection anomaly over the equatorial western Pacific. Furthermore, the relatively westward-extended SST warming can ultimately be traced back to the preceding multi-year La Niña through the chain of causation involving weak nonlinear dynamical cooling, weak anomalous subsurface temperature gradients, and abundant warm water accumulation in the western Pacific. This mechanism similarly explains other El Niño events following multi-year La Niña, especially the 2009 event, providing insights into the rare transition from a multi-year La Niña to a strong El Niño. However, current climate models demonstrate limited skill in simulating 2023-like El Niño events and associated mechanisms, primarily due to the systematic biases in the zonal distributions of SST and convection anomalies. Our proposed mechanism, rooted in tropical Pacific dynamics, offers a new perspective to improve model simulations and predictions of such events.

INTRODUCTION

El Niño-Southern Oscillation (ENSO) events are of great spatial and temporal complexities and exhibit notable differences among themselves.[1,2] The El Niño event in 2023 was rather extraordinary, which featured three distinct aspects. First, prior to this El Niño event, there was a triple-dip La Niña event,[3–5] recharging the warm water volume (WWV)[6] in the equatorial Pacific during the preceding winter to its maximum value since 1980.[7] Second, despite the first-ranked WWV pre-condition of this event, its peak intensity of the Niño3.4 index was placed 4th behind the 1982, 1997, and 2015 El Niño events (Figure S1A) and merely reached the extreme category.[8,9] Third and most remarkably, despite sufficiently strong warm sea surface temperature (SST) anomalies in the equatorial central-eastern Pacific, the westerly wind anomalies were surprisingly weak, presenting a rare characteristic of strong oceanic signal but weak atmospheric signal of ENSO, or saying, a "strong El Niño but weak Southern Oscillation".

The primary reason that the 2023 event failed to reach the unprecedented intensity suggested by WWV was a lack of synchronization in atmospheric conditions, which has been identified as "ocean-atmosphere decoupling".[10,11] Since the tropical Pacific SST warming seemingly contradicts the absence of westerly winds, several studies have offered explanations based on the factors outside the tropical Pacific dynamics. For instance, Hong et al.[12] suggested that the North Atlantic Tripole and the extratropical North Pacific extreme SSTs could trigger negative North Pacific Meridional Mode (NPMM) activities and easterly anomalies, thereby weakening the SST-wind coupling during the development stages of El Niño. Using the Community Earth System Model (CESM), Hu et al.[10] carried out a series of sensitivity prediction experiments and concluded that the record-breaking pantropical warming in 2023 mitigated this El Niño. Zhao et al.[13] argued that the enhanced precipitation over the Indian summer monsoon region and tropical North Atlantic overwhelmed the effect of the El Niño induced westerlies, resulting in the easterly anomalies. Meanwhile, Kim et al.[14] emphasized that the unusual easterly anomalies over the tropical western-central Pacific, which hindered the development of El Niño, were associated with a prominent east-west SST gradient. This gradient could be further attributed to a negative NPMM[15] and a deepened thermocline over the Philippine Sea. Despite all these potential explanations, if the "ocean-atmosphere decoupling" observed in this event was driven by factors unrelated to the tropical Pacific as the above studies suggested, a critical question emerges: was the weak Southern Oscillation during the 2023 El Niño event merely coincidental and inherently unpredictable?

However, the unique 2023 El Niño was preceded by another rare triple-dip La Niña event, raising questions about a potential connection between these two unusual ENSO events. Previous studies have noted that multi-year La Niña events in observations rarely transition into strong El Niño, and that none of the three extreme El Niño events in recent decades (1982, 1997, and 2015) followed multi-year La Niña,[11,16] implying that the weaker-than-expected intensity of the 2023 El Niño event might be associated with the multi-year La Niña preconditioning instead of mere coincidence. Mechanistically, they proposed that the lingering cold state in the central Pacific from the multi-year La Niña hindered the eastward movement of deep atmospheric convection, delaying ocean-atmosphere coupling and thus impeding the development of El Niño. This explanation aligns with the interpretation proposed by Kim et al.[14] and holds validity until SST anomalies turned positive. Yet, it should be noted that even the central-to-eastern Pacific SSTs warmed after May 2023, weak westerly wind anomalies persisted until October. Evidently, the reason for the "ocean-atmosphere decoupling" phenomenon in 2023, especially the lack of robust westerly anomalies despite SST warming, needs to be further clarified to provide a potential pathway to improving the prediction of future analogous events.

MATERIALS AND METHODS

Observational data

The monthly mean datasets used in this study include: (1) the SST data from the Extended Reconstructed SST version 5 (ERSSTv5),[17] Hadley Centre Sea Ice and Sea Surface Temperature data set (HadISST),[18] and Center Centennial in situ Observation-Based Estimates SST 2 (COBE SST2);[19] (2) the precipitation data from the Global Precipitation Climatology Project Monthly Analysis Product (GPCP)[20] and CPC Merged Analysis of Precipitation (CMAP);[21] (3) the surface (10 m) wind data from the National Centers for

Environmental Prediction–Department of Energy Reanalysis 2 (NCEP2),[22] the fifth generation ECMWF reanalysis (ERA5),[23] and Japanese 55-year Reanalysis (JRA55);[24] (4) the surface heat flux data from the NCEP2, ERA5, Global Ocean Data Assimilation System (GODAS),[25] Ocean Reanalysis System 5 (ORAS5),[26] and Estimating the Circulation and Climate of the Ocean 2 (ECCO2);[27] and (5) the subsurface oceanic fields, including potential temperature and three-dimension currents, from the GODAS, ORAS5, and ECCO2. The analysis period spans from 1980 onwards, with the exception of ECCO2, which begins from 1992. All anomalies in this study are calculated as the differences by subtracting the climatological seasonal cycle for the most recent 30-year base period from 1991 to 2020 (29-year period from 1992 to 2020 for the ECCO2).

Definitions of indices

Several indices based on previous studies and new definitions are used in this study. The Niño3.4 SST index, the most common ENSO indicator, is calculated as the average of SST anomalies in the Niño3.4 region (170°W–120°W, 5°S–5°N). The Pr_tropics index, used for quantifying convection anomaly, is defined as the mean precipitation anomaly in the region of 160°E–120°W, 5°S–5°N. Another convection anomaly index Pr_WP is defined as the mean precipitation anomaly in the far western Pacific (120°–160°E, 5°S–5°N). The U_ Niño4 index is defined as the mean surface zonal wind anomaly in the Niño4 region. The warm water volume (WWV) index, widely used for measuring equatorial Pacific heat content, is defined as the water volume above the 20°C isotherm in the region of 120°E–80°W, 5°S–5°N.[6] To show the accumulation of warm water in the western Pacific, an WWV_west index is defined similarly to the WWV index, but calculated in the region of 120°E–170°W, 10°S–10°N.

An SST westward extension index (SST_wb) is defined as

$$SST\_wb = 200^{\circ} - \int_{135^{\circ}}^{200^{\circ}} bool(T' > 0^{\circ}C)dx \tag{1}$$

where T' is SST anomalies, and 135° and 200° (160°W) represent the eastern and western boundaries of the typical longitudinal range of the SST warming western boundary. The Boolean function equals 1 when the condition is satisfied and 0 otherwise. A similar index is defined to characterize the westward extension of anomalous convection:

$$Pr\_wb = 185^{\circ} - \int_{120^{\circ}}^{185^{\circ}} bool(Pr' > 0mm)dx \tag{2}$$

where Pr' denotes precipitation anomalies, and the remaining parameters are defined analogously to those in Eq. (1).

Mixed layer heat budget analysis

To diagnose the dynamic and thermodynamic processes through which the monsoon affects the development of subsequent ENSO, a heat budget analysis for mixed-layer temperature anomalies is conducted. Following previous studies,[28,29] the budget difference equation can be written as:

$$\begin{aligned}\frac{\partial T'}{\partial t} = & \underbrace{\underbrace{-u'\frac{\partial \overline{T}}{\partial x}}_{UA}\underbrace{-v'\frac{\partial \overline{T}}{\partial y}}_{VA}\underbrace{-w'\frac{\partial \overline{T}}{\partial z}}_{EK}\underbrace{-\overline{u}\frac{\partial T'}{\partial x}}_{UM}\underbrace{-\overline{v}\frac{\partial T'}{\partial y}}_{VM}\underbrace{-\overline{w}\frac{\partial T'}{\partial z}}_{TH}}_{D\_l} \\ & \underbrace{-\left(u'\frac{\partial T'}{\partial x}+v'\frac{\partial T'}{\partial y}+w'\frac{\partial T'}{\partial z}\right)}_{D\_nl}+\frac{Q'_{net}}{\rho_0 C_p H}+R\end{aligned} \tag{3}$$

where $\overline{()}$ means the climatological annual cycle, and $(\ )'$ means monthly mean anomalies. The terms T, u and v represent the mean temperature, as well as the zonal and meridional ocean currents within the mixed layer, respectively. w denotes the vertical current at the bottom of the mixed layer. Q'_{net} is the net surface heat flux anomaly into the ocean. $\rho_0 C_p$ is the specific heat capacity per unit volume, where the seawater density ρ_0 is 1.03 × 10^3 Kg m^{-3}, and the specific heat capacity C_p is 4000 J kg^{-1} K^{-1}. H is the mixed layer depth defined as the depth where the subsurface temperature differs from the surface (5 m) temperature by 0.8°C. Note that, dynamical processes are calculated using a fixed subsurface depth of 50 m to be consistent with the mathematical basis of the temperature advection equation, whereas the temporal variations of mixed-layer depth are considered for the thermodynamical term as surface heat flux penetrates and warms up the whole mixed layer. R is the residual term.

On the right side of Eq. (1), the first three terms denote the advection of mean temperature by the anomalous ocean current, which can generate zonal advection (*UA*), meridional advection (*VA*), and the Ekman pumping (*EK*) respectively. The next two terms represent the redistribution of anomalous temperature by the mean zonal (*UM*) and meridional (*VM*) ocean currents. The advection of anomalous temperature by the mean vertical ocean current is the thermocline feedback (*TH*). All these six terms are linear dynamical processes. The last three terms, nonlinear dynamical heating, are the combined effects of anomalous ocean currents and anomalous temperature gradients.

Figure S2 shows the downward heat flux anomalies from five different datasets, including GODAS, NCEP2, ERA5, ORAS5, and ECCO2. The GODAS heat flux is simulated based on NCEP2 data, and the two are highly similar (Figures S2A–H). However, they clearly do not align well with the overall patterns of sea surface temperature (SST), precipitation, and wind fields. In contrast, the ERA5 heat flux data are more reasonable and also serve as the benchmark for the two newer datasets, ORAS5 and ECCO2, with significant similarities among the three (Figures S2I–S). Therefore, we replaced the GODAS heat flux data with ERA5 data for the heat budget calculations.

CESM1 piControl simulation and events definitions

Two long-term control simulations under the pre-industry greenhouse gas concentration from the Community Earth System Model versions 1 and 2 (CESM1 piControl and CESM2 piControl)[30,31] are used to evaluate the performance of coupled climate model in simulating the phenomenon of a "strong El Niño but weak Southern Oscillation" following multi-year La Niña. This CESM1 simulation, which was run on a roughly 1° horizontal grid for 2200 model years, is publicly available from years 400 to 2200. The CESM2 simulation, which has the identical resolution, spans years 1 to 1200, with the latter 800 years being utilized in this study. Both simulations have been widely used to study ENSO and related ocean-atmospheric processes, demonstrating decently good performance in simulating these phenomena.[32,33,34]

Multi-year La Niña events in the simulation are identified when the Niño3.4 is lower than -0.5 standard deviations for two or more consecutive DJF seasons. Strong El Niño events are defined as those with a DJF Niño3.4 higher than 2 standard deviations. Strong El Niño events in the simulation are further categorized into two groups: those preceded by multi-year La Niña and those preceded by ENSO-neutral state (defined as an absolute value of the DJF Niño3.4 index lower than 0.5 standard deviations).

Atmospheric general circulation model experiments

In this study, we utilized the Community Atmospheric Model version 6/5 (CAM6/CAM5),[35,36] the atmospheric component of the Community Earth System Model version 2.2.0/1.2.2 (CESM2.2.0/CESM1.2.2) developed by the National Center for Atmospheric Research, to conduct experiments forced by SST anomalies. The CAM6/5 experiments were carried out with a horizonal resolution of 0.9° latitude×1.25° longitude (f09)/1.9° latitude×2.5° longitude (f19) and a vertical resolution of 32/30 levels.

Three experiments are conducted parallelly using CAM6 and CAM5. Initially, a control-run experiment (referred to as CTRL), which was driven by the climatological annual cycle of SST, was integrated for 30 years. Subsequently, the SST anomalies in the equatorial Pacific (120°E–80°W, 10°S–10°N) during the summers (from May to September) of 2023 and 1997 were separately superimposed onto the SST forcings for two sensitivity experiments. Analogous to the CTRL, each of the sensitivity experiments was integrated for 30 years. For all experiments, the initial 10-year period was used for model spin-up. To investigate the impacts of SST anomalies, in the last 20-year period, we subtracted the results of the CTRL from those of the two sensitivity experiments.

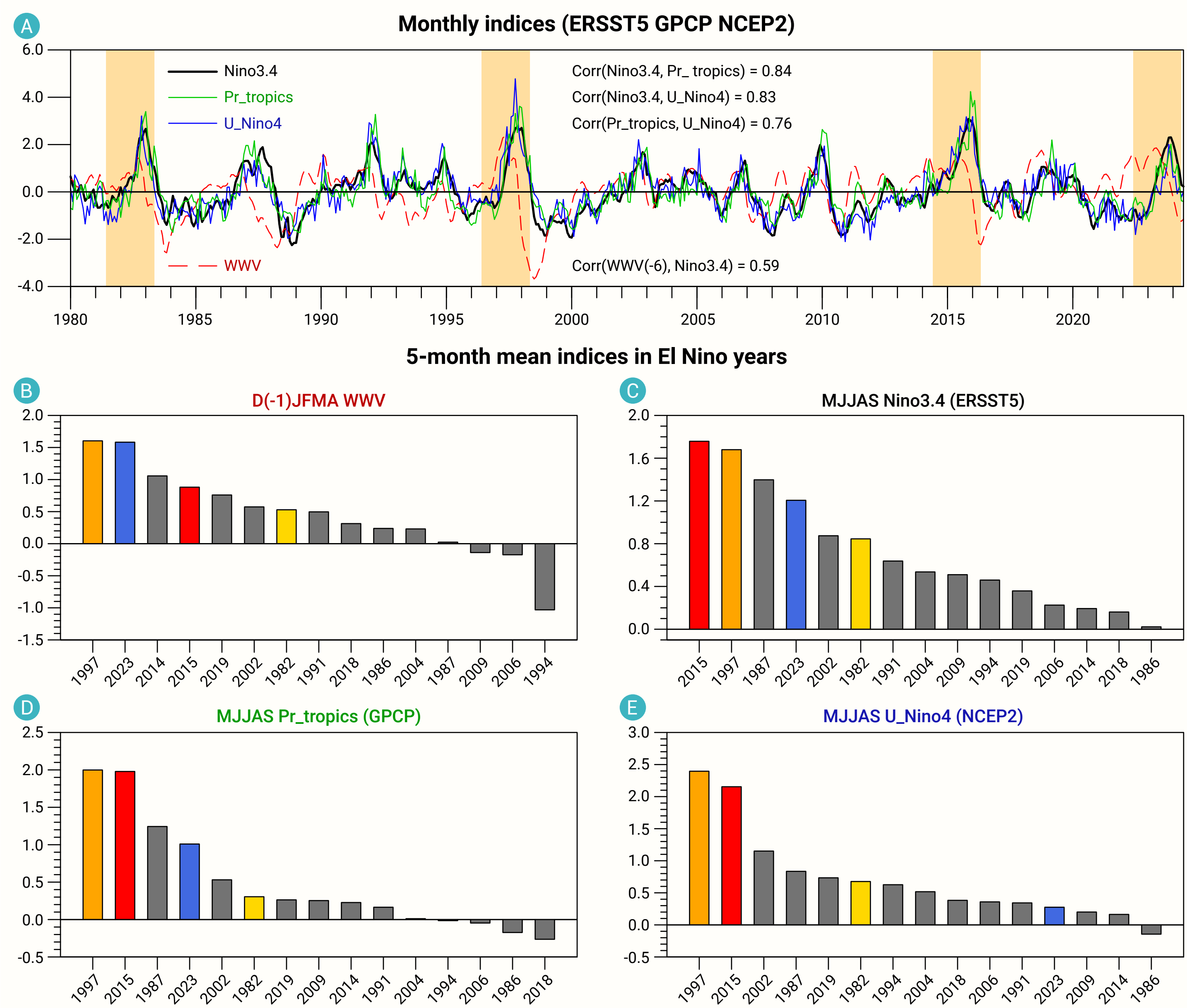

Figure 1. The strong El Niño but weak Southern Oscillation in 2023 (A) Monthly time-series of warm water volume (WWV), Niño3.4, tropical Pacific precipitation (Pr_tropics), and Niño4-mean zonal wind anomalies (U_Niño4) indices from 1980 to 2024. The panel presents the correlation coefficients between WWV (with a 6-month lead) and Niño3.4, Niño3.4 and Pr_tropics, Niño3.4 and U_Niño4, as well as Pr_tropics and U_Niño4, which are 0.59, 0.84, 0.83, and 0.76 respectively. The orange shadings denote the three extreme El Niño events and the 2023 El Niño event. (B)–(E) 5-month mean indices of December(-1) to April WWV (B), May to September (MJJAS) Niño3.4 (C), MJJAS Pr_tropics (D), and MJJAS U_Niño4 (E) of El Niño events, arranged in descending order of each index. Notably, in 2023, the MJJAS U_Niño4 index ranked 12th, while both the MJJAS Niño3.4 and the Pr_tropics indices ranked 4th in their respective series. Note that all the indices have been standardized from 1980 to 2024.

Linear baroclinic model experiments

A linear baroclinic model (LBM)[37] was employed to explore the surface wind response to the anomalous heating in El Niño events. The LBM is a primitive equation model, which is linearized based on the observed climatology derived from the NCEP–DOE Reanalysis over the period from 1991 to 2020. We employed a version of the LBM with a T42 horizontal resolution and 20 sigma levels in vertical resolution. Two sets of LBM experiments were conducted, where the forcing was prescribed to anomalous heating during the summers (from May to September) of 2023 and 1997. Each of the LBM experiments was integrated for 30 days. To obtain a steady-state response to the anomalous atmospheric heating, the results from the last 10 days were averaged.

RESULTS

Weak Southern Oscillation during the 2023 strong El Niño

The charging of WWV often indicates that SST warming in the equatorial central-eastern Pacific, i.e., an El Niño event may occur 6 to 12 months later (Figure 1A).[6,38] El Niño, as an oceanic phenomenon, generally occurs in conjunction with the atmospheric phenomenon-Southern Oscillation.[39,40] In particular, the zonal non-uniform SST warming causes eastward shift of the convection center, which creates an east-west anomalous sea level pressure gradient and further leads to the occurrence of westerly wind anomalies (Figure 1A).[41] Subsequently, the westerly wind anomalies induce subsurface oceanic processes, including zonal advection and eastward-propagating Kelvin waves, which in return enhance the SST warming, forming the so-called Bjerknes feedback.[42]

Such ocean-atmosphere coupling processes are crucial for the development of El Niño and typically prominent in extreme events. During the development of three extreme El Niño events in 1982, 1997 and 2015, the indices (see MATERIALS AND METHODS) of ENSO-related equatorial SST anomaly (Niño3.4), convection anomaly (Pr_tropics), and zonal wind anomaly (U_Niño4) were highly synchronic seasonally (Figures 1C–E) and monthly (Figures S1B–D). The three indices in the summers of 1997 and 2015 were ranked top two across all El Niño events, showing an exceedingly robust ocean-atmosphere coupling relationship. In 1982, owing to its relatively belated onset, the three aforementioned indices during summer were ranked 6th. Although the magnitudes of these indices in the 1982 summer were not exceptionally high, they still remained within the leading ranks and followed a coherent ocean-atmosphere coupling relationship (Figures 1C–E). However, an unexpected situation occurred in 2023. While the Niño3.4 and Pr_tropics indices both ranked 4th in summer, the U_ Niño4 index only ranked 12th, far behind the other two indices (Figures 1C–E).

The monthly evolutions of the three indices more detailly reveal the differences in ocean-atmosphere coupling processes between the 2023 El Niño events and the three extreme ones (Figures S1B–E). Corresponding to the early-onset SST warming, the westerly anomalies in 1997 and 2015 occurred at the beginning of the year and gradually intensified as the SST further warmed up (Figures S1B–C). In 1982, due to the relatively late onset of warm SST, westerly wind anomalies did not appear in the early months of the year. However, by summer, as SST warming emerged alongside a positive convection anomaly in the central-eastern Pacific, westerly wind anomalies developed. This progression highlighted a remarkable synchrony among the three indices that year (Figure S1D). In 2023, after May, when the equatorial central-eastern Pacific SST anomalies switched from negative to positive, the positive convection anomaly occurred accordingly. Yet, the zonal wind anomalies persisted in a weak state until September, which, in turn, led to the El Niño event missing the opportunity to reach a more elevated intensity in that year (Figure S1E). That is, the warm SST has induced a positive convection anomaly through the typical ocean-atmosphere coupling mechanism. However, this positive convection anomaly has not further triggered westerly wind anomalies as in most cases. Apparently, the coupling chain broke down between convection and wind rather than between SST and convection, which is different from the situation of a weak linkage between SST and convection during the so-called "uncoupled El Niño" in the previous studies.[43,44] Thus, simply characterizing the 2023 situation as "ocean-atmosphere decoupling" might be insufficiently accurate.

Relatively westward SST warming leading to weak westerly anomalies

The next question is: why did the anticipated strong westerly anomalies not occur? In the presence of a pronounced convection anomaly, it seems that the ocean-atmosphere state within the equatorial Pacific struggled to explain the weak westerly anomalies. Thus, it is fair to hypothesize that factors beyond the tropical Pacific might have played certain roles[10,12,14]. However, by carefully reexamining the differences between 2023 and the three extreme El Niño events, we posit that the key reason for the weak westerly anomalies may lie in the zonal distribution of warm SST anomalies in the equatorial Pacific.

In 2023, a record-breaking coastal El Niño took place.[45,46] As a result, the most pronounced warm SST anomalies were concentrated in the eastern Pacific, which naturally drew our attention to this region. Indeed, when focusing on the central-eastern Pacific, the 2023 El Niño seems to be roughly identical to the three extreme events (Figures 2A–D). However, if we focus only on the regions with significant SST anomalies, we may miss an overlooked feature on the western side in 2023. Throughout this year, the warm SST anomalies persistently expanded to 150°E or even further westward, accompanied by relatively milder cold SST anomalies in the far western Pacific (Figure 2D). In contrast, during the development of the three extreme El Niño events, the western boundaries of their warm SST anomalies gradually retreated eastward towards the Date Line (Figures 2A–C). This difference in the zonal distribution of SST anomalies was seemingly inconspicuous, but actually exerted a substantial impact and might well be the primary cause of the weak westerly anomalies observed in the summer of 2023.

The westward-extended warm SST anomalies not only caused the positive convection anomaly to expand westward but also diminished the intensity of the negative convection anomaly in the far western Pacific (Figure 2H). Conversely, during the three extreme El Niño events, the negative convection anomalies on the west were remarkably strong (Figures 2E–G). These anomalies, in combination with the positive convection anomalies in the east, efficiently formed an anomalous zonal-overturning circulation cell (the so-called Walker circulation cell), promoting the generation of easterly anomalies at the upper levels, and westerly anomalies at the lower levels (Figures 2I–K). In 2023, the positive convection anomaly was prevalent across nearly the entire zonal expanse of the equatorial Pacific, and the negative convection anomaly in the western Pacific was extremely weak. As a result, it was difficult to establish a strong anomalous Walker circulation cell (Figure 2L). Note that, in this year, the atmospheric ascending in the western Pacific was compensated by meridional convergence (Figure 2P), which is also different from the patterns observed during the three extreme El Niño events (Figures 2M–O). The relatively westward-extended positive SST and convection anomalies leading to weak westerly wind anomalies can be verified by more general evidence. In July 1997 and June 2015 when the positive convection anomalies underwent an occasional westward expansion, there was a marked disruption in the westerly wind anomalies in the equatorial Pacific (Figures 2J–K). Moreover, although the convection anomaly in 2023 was stronger than that in 1982, the westerly anomalies were, on the contrary, weaker (Figures 2I& L). The above-mentioned zonal distributions of oceanic and atmospheric variables are further validated by different sources of datasets (Figure S3). In short, a stronger positive convection anomaly does not necessarily induce stronger westerly anomalies. Instead, the co-occurrence of positive and negative convection centers in the zonal direction is crucial for triggering strong westerly anomalies.

To quantitatively support the above interpretation, Figure 3 summarizes the relationships between westerly wind anomalies and different characteristics of SST and convection anomalies during years when the Niño3.4 index exceeds 0.5 standard deviations (Table S1). Although the U_ Niño4 index shows high correlations with the Niño3.4 and Pr_tropics indices when all years are included, these relationships are largely controlled by the two extreme El Niño events in 1997 and 2015. Once these years are excluded, the correlations become weak, indicating that the amplitude of SST warming or basin-mean convection alone is insufficient to explain westerly wind variability during non-extreme events (Figures 3A–B). In contrast, indices describing the westward extension of SST warming and convection, particularly SST_wb and Pr_wb (see MATERIALS AND METHODS), retain moderate correlations with the WW index, even after excluding extreme years (Figures 3C–D). Moreover, precipitation anomalies over the far western Pacific (Pr_WP, see MATERIALS AND METHODS) exhibit a strong correlation with the U_ Niño4 index (Figure 3E), emphasizing the importance of suppressed convection in the far western Pacific. These results suggest that the zonal structure of SST and convection anomalies, rather than their overall intensity, plays a key role in regulating westerly wind anomalies.

To further examine the above speculation that the relatively westward-extended SST warming led to zonally uniform convection and weak westerly anomalies in 2023, we conducted two sets of atmospheric model experiments using the Community Atmospheric Model version 6 (CAM6; see MATERIALS AND METHODS), which were respectively forced by SST anomalies in the 2023 and 1997 summers (from May to September, Figures 4A–B). The results show that the more westward-extended SST warming in 2023 induced a more westward extended precipitation response and weaker westerly anomalies compared to the response to the 1997 SST warming (Figure 4C). However, both experiments simulated dipole-shaped precipitation responses, with a strong negative center over the Maritime Continent to the west of positive center (Figures 4A–B), which closely resembled the observed anomalous precipitation pattern in the 1997 summer. These dipole precipitation responses, as it should, led to overestimation of the westerly wind responses in the two experiments, especially in the 2023 experiment. In reality, the 2023 precipitation anomaly was strikingly different from that in 1997, with a weak negative center near the Maritime Continent and a stronger positive center located in the central Pacific, rather than the eastern Pacific as seen in 1997 (Figures 4G–H). That is, the precipitation and wind responses in the CAM6 experiment forced by the 2023 SST anomalies may not be sufficiently accurate. However, compared to its previous version CAM5, CAM6 already demonstrates significant improvements. CAM5 tends to produce an unrealistic meridional dipole pattern in precipitation over the Maritime Continent and the subtropical northwestern Pacific, while also exhibiting an overly sensitive precipitation response in the eastern Pacific. As a result, in CAM5, the 2023 warm SSTs trigger excessively strong westerly wind anomalies (Figure 4D), although these responses are considerably weaker compared to those in the CAM5 1997 experiment (Figures 4E–F). These model biases will

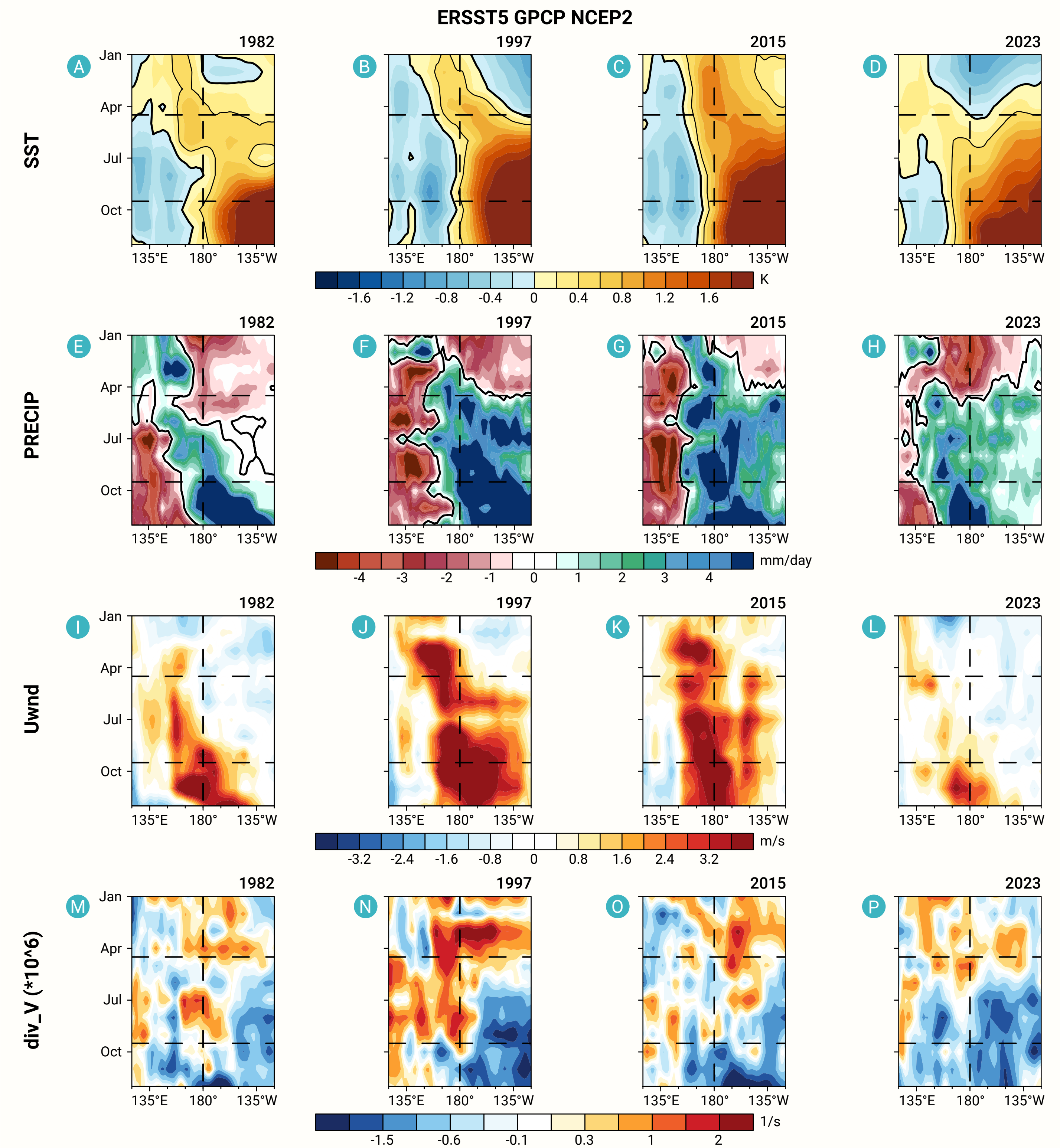

Figure 2. Different zonal distribution of ocean-atmosphere variables in the equatorial Pacific between the three extreme El Niño events and the 2023 El Niño event (A)–(D) Hovmöller diagrams of the equatorial (5°S–5°N) mean SST anomalies (shaded) in the 1982 (A), 1997 (B), 2015 (C), and 2023 (D) El Niño events. The zero and 0.4 lines are highlighted as contours. (E)–(H) Similar to (A)–(D), but showing precipitation anomalies (shaded), with the zero lines as contours. (I)–(L) Similar to (A)–(D), but showing surface zonal wind anomalies. (M)–(P) Similar to (A)–(D), but showing surface meridional wind divergence. The two horizontal dashed lines demarcate the time-period from May to September, while the vertical dashed line indicates the 180° longitude.

be discussed in more details in the Discussion.

To explore how winds respond to actual precipitation patterns, we employed a linear baroclinic model (LBM, see MATERIALS AND METHODS) to conduct two sets of experiments with forcings from the observed anomalous atmospheric heating in the 2023 and 1997 summers (Figures 4J–K). With realistic spatial patterns, the 2023 heating induced a weak westerly wind response to the west of the Dateline, whereas the 1997 heating caused a stronger westerly wind response extending to 120°W (Figures 4J–K). The differences between the two LBM experiments reveal a distinct pattern of the weaker westerly wind anomalies in the case of 2023 event (Figure 4L). The

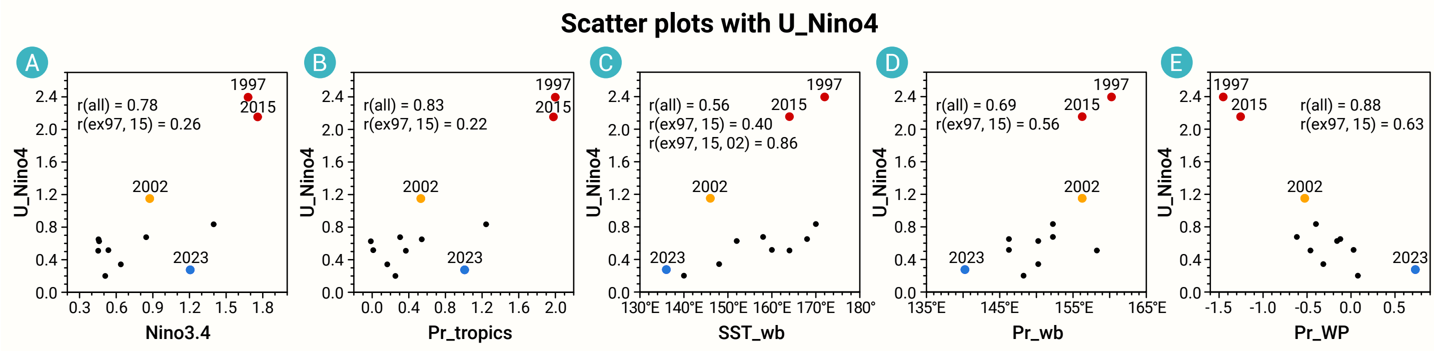

Figure 3. Relationships between westerly wind anomalies and the zonal extent of SST and convection Scatter plots showing the relationships between the MJJAS U_Niño4 index (y-axis) and (A) the Niño-3.4 index, (B) the tropical mean precipitation index (Pr_tropics), (C) the SST westward extension index (SST_wb), (D) the precipitation westward extension index (Pr_wb), and (E) precipitation anomalies over the western Pacific (Pr_WP) on the x-axis. Both the overall correlation coefficients and those calculated with selected years excluded are indicated in each panel. Note that all the indices have been standardized from 1980 to 2024.

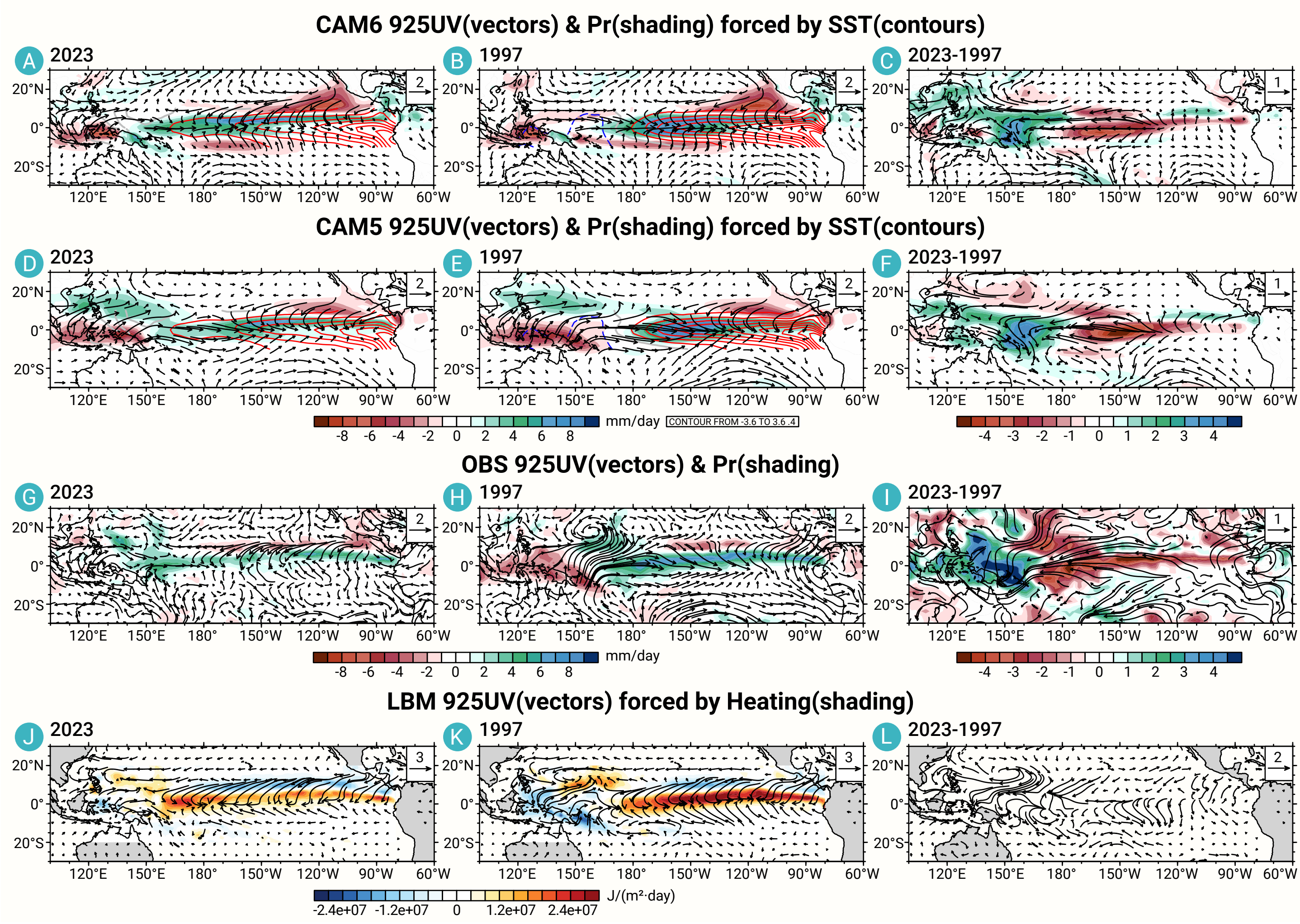

Figure 4. Forcings and responses of the model experiments and corresponding observed patterns (A)–(B) The responses of precipitation (shading) and 925hPa winds (vectors) of the CAM6 experiments forced by the SST anomalies (contours) during the summers (from May to September) of 2023 (A) and 1997 (B). (C) The differences in the responses between the two CAM6 experiments (2023 minus 1997). (D)–(F) Similar to (A)–(C), but showing the results of CAM5. (G)–(H) The observed anomalous precipitation (shading) and 925hPa winds (vectors) patterns during the summers (from May to September) of 2023 (G) and 1997 (H). (I) The differences in precipitation and 925hPa winds between 2023 and 1997 (2023 minus 1997). (J)–(K) The responses of 925hPa winds (vectors) of the LBM experiments forced by the atmospheric heating anomalies (shading) during the summers (from May to September) of 2023 (J) and 1997 (K). (L) The differences in the responses between the two LBM experiments (2023 minus 1997).

above model results confirm that a strong dipole pattern of convection anomalies has the potential to trigger strong westerly anomalies, while a zonally uniform pattern has limited capability in doing so. In addition, the systematic bias in moist convection within convection-permitting atmospheric general circulation models can result in inaccurate precipitation and surface wind responses to SST forcing, which may partly explain the overestimation of El Niño prediction in the early 2023.[14]

Weak nonlinear cooling favoring SST warming in the western Pacific

A mixed layer ocean heat budget analysis is conducted to diagnose the excessive SST warming towards the western Pacific in 2023. It should be noted that due to the biases in heat flux term, we combined the subsurface oceanic fields from the Global Ocean Data Assimilation System and heat flux fields from the fifth generation ECMWF reanalysis for the heat budget analysis. More details are described in the see MATERIALS AND METHODS.

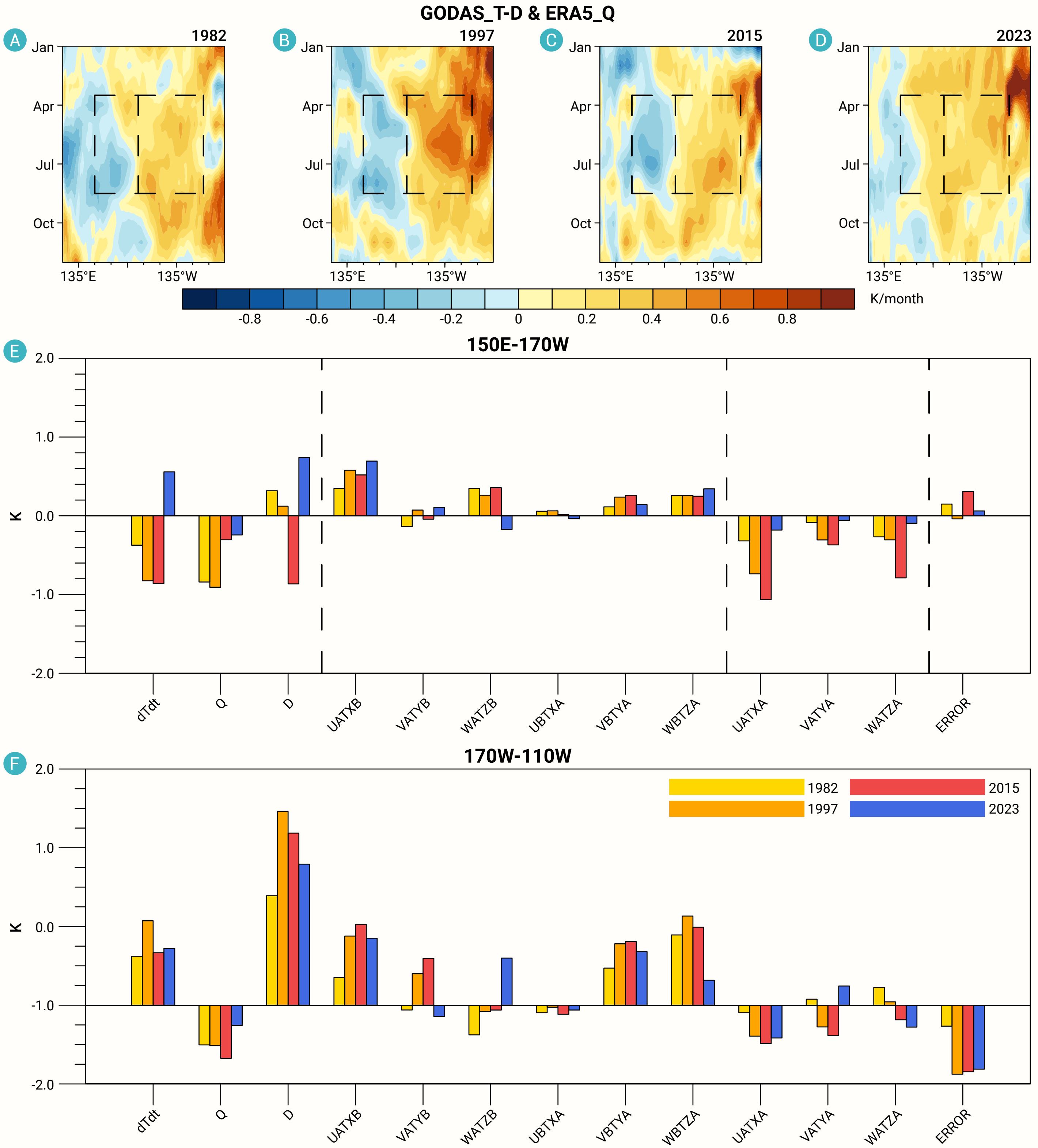

Figure 5. Mixed layer heat budget analysis across three longitudinal ranges in the equatorial Pacific (A)–(D) Hovmöller diagrams of the equatorial (5°S–5°N) mean mixed layer temperature tendency (shaded) in the 1982 (A), 1997 (B), 2015 (C), and 2023 (D) El Niño events. The left box demarcates the longitudinal range of 150°E–170°W, and time range between April and August. The right box demarcates the longitudinal range of 170°E–110°W, and same time range. (E) Mixed layer heat budget tendency budget analysis from April to August of the four El Niño events in the region of 150°E–170°W, 5°S–5°N. Bars from left to right are "dTdt" temperature tendency, "Q" net heat flux, "D" the total dynamical effect, six linear dynamical processes, three nonlinear dynamical processes, and "R" the risidual term (R=dT/dt - Q - D). (F) Similar to (E), presenting the results in the regions of 170°–110°W, 5°S–5°N.

Similar to the case of SST anomalies, the 2023 El Niño event displayed a different zonal distribution of mixed layer temperature tendency evolution in the equatorial Pacific from those during the three extreme El Niño events (Figures 5A–D). In the three extreme El Niño events, the temperature tendency exhibited a dipole pattern of cooling in the west and warming in the east, with the Date Line serving as the boundary. On the other hand, in 2023, the cooling tendency in the west was weaker and the warming tendency extended westward approximately to 150°E. Plainly speaking, within the longitudinal range of 150°E–170°W, the three extreme El Niño events experienced cooling during their development, whereas the 2023 El Niño event exhibited warming. Therefore, the heat budget analysis terms from spring to summer (from March to August) are averaged within 150°E–170°W, 5°S–5°N (defined as region WP hereafter) to reveal the reason for the relatively westward extension of equatorial SST warming in 2023 (Figure 5E). Additionally, another longitudinal range to the east (170°W–110°W, C-EP hereafter) where the temperature tendencies were similar among the four events are defined to verify the heat budget analysis (Figure 5F).

In the C-EP region, not only is the temperature tendency term similar, but the heat budget terms are also physically consistent across the four El Niño events (Figure 5F). Specifically, zonal advection ($u'\frac{\partial \overline{T}}{\partial x}$), thermocline feedback ($\overline{w}\frac{\partial T'}{\partial z}$) and meridional heat redistribution ($\overline{v}\frac{\partial T'}{\partial y}$) processes are the major positive contributing factors, while the impacts of other terms are relatively minor. It should be noted that the relatively large residual partly arises from unresolved processes such as vertical mixing and entrainment, as well as accumulated uncertainties among large-magnitude terms. As these effects are common to all four events, they do not affect the robustness of the inter-event comparison. Despite certain biases, the heat budget analysis in this regions validates the robustness of our calculations as it shows the dominant roles of thermocline feedback term and zonal advection term in promoting C-EP warming, which conforms to the intrinsic physical features in the equatorial Pacific.[47,48] More importantly, it indicates that, compared with the three extreme events, the 2023 El Niño was not exceptional in terms of mechanism in the large SST warming region.

In the WP region, 2023 El Niño featured a positive temperature tendency, which was distinct from the negative tendencies in the other three extreme El Niño events (Figure 5D). Nevertheless, the three main positive terms (zonal advection, thermocline feedback, and meridional heat redistribution) in the C-EP region acted comparably in all the four events in promoting SST warming within this region. Moreover, the Ekman pumping effect ($w'\frac{\partial \overline{T}}{\partial z}$) contributed positively in the other three events but a negative one in 2023, resulting in a smaller sum of linear dynamical terms in that year. These findings present a dilemma: In 2023, despite the positive tendency, the warming-favored processes were rather weaker compared to the three events with negative tendencies. This disparity suggests the need to examine the effects of other factors. Given the negative tendencies in the three extreme events, it is reasonable to infer the existence of negatively contributing factors. In fact, the nonlinear dynamical processes played this role, causing cooling across all dimensions in the WP during those events (Figures 2E & S4A–I). However, in 2023, this nonlinear cooling effect did not occur in the WP region, which accounts for the local positive temperature tendency (Figures 2E & S4J–L). In other words, the absence of nonlinear cooling processes is the dominant contributor to the relatively westward expansion of SST warming during the 2023 El Niño event. Considering the uncertainties in the reanalysis products, the same ocean heat budget analysis was performed with two additional datasets (ORAS5, Figures S5–S6; ECCO2, Figures S7–S8). The high level of agreement among these results verifies the robustness of the analysis and the ensuing interpretation

Exceptional western Pacific WWV inhibiting nonlinear cooling effects

Nonlinear dynamical processes are the combined effects of anomalous ocean currents and anomalous temperature gradients. So, what factors contributed to the pronounced nonlinear cooling in the western Pacific during the three extreme El Niño events, while only a weak nonlinear cooling occurred in 2023? Figures S9–S10 display the bimonthly evolutions of subsurface anomalous temperature and currents during the four El Niño events. While the anomalous currents in 2023 were similar to those in the three extreme El Niño cases, the temperature distribution was strikingly different in that year. At the beginning of the three extreme years, cold temperature anomalies had already emerged in the western Pacific and off the equator (Figures 2A–D). With the further decrease in the WWV in the western Pacific (WWV_west, see MATERIALS AND METHODS), anomalous temperature gradients in all three dimensions persisted throughout the three extreme El Niño years (Figures 6A–C). Therefore, the anomalous eastward zonal currents, equatorward meridional currents and vertical currents in the WP region induced substantial in-situ nonlinear cooling (Figures S4A–I), restricting the westward extension of SST warming during these years.

Before the onset of the 2023 El Niño, a large amount of warm water had accumulated in the western Pacific due to the previous triple-dip La Niña. When the anomalous zonal currents and mean meridional ones began to transport mass and heat away from the western Pacific and the equator, the WP region remained with broad and uniform subsurface warming, resulting in weak anomalous temperature gradients until the WWV_west switched to negative after September (Figures 6D & S4J–L). Thus, the equatorial SST warming in 2023 started to retreat eastward since September (Figure 2D), favoring the occurrence of westerly wind anomalies after that (Figure 2L). In fact, the WWV_west was high not only after the 2020–2022 triple-dip La Niña but also after the other multi-year La Niña events (Figure 6E). In this case, we suggest that the relatively westward-extended SST warming in 2023, induced by weak nonlinear dynamical cooling in the WP region and resulting in the prevention of westerly anomalies generation, might not be entirely accidental or inimitable. Similarly, all the above analyses are validated with the ORAS5 and ECCO2 datasets (Figures S11–S16).

CONCLUSION and DISCUSSION

In the conventional ENSO recharge framework, multi-year La Niña events are expected to have a higher probability of transitioning to strong El Niño than single-year La Niñas as they more persistently recharge the ocean heat content toward the equator via Sverdrup transport.[6,15] However, only the 2020-2022 multi-year La Niña event evolved into a relatively strong El Niño. In contrast, other multi-year La Niña events merely transitioned to a moderate El Niño or nearly an ENSO-neutral conditions (Figures S17A–D). Even the 2023 El Niño failed to reach the intensity predicted by its second-highest WWV precondition. Given the typical nature of the 2023 El Niño, the findings from this analysis may provide insights into why strong El Niño events are rare following multi-year La Niña events.

In the summer of 2023, strong SST warming in the equatorial central-eastern Pacific triggered a corresponding positive convection anomaly. However, the relatively westward extension of this warming pattern led to zonally uniform ascending across the equatorial Pacific, which was inconducive to the formation of westerly wind anomalies. This westward shifted SST warming, coupled with a zonally uniform positive convection anomaly and weak westerly anomalies, was also observed in other post-multi-year La Niña years, despite inter-event differences (Figure S17), which is insensitive to the choices of datasets (Figure S18). Notably, the 2009 event shares striking similarities with the 2023 El Niño. In 2009, SST warming extended westward to around 150°E, and positive convection reached 135°E, generating weak westerly anomalies over the western Pacific (Figures S17C, G, K & O). Quantitatively, the Pr_tropics ranked 8^{th}, closely matching the 9^{th} Niño3.4 index, but accompanied by the unmatched and lower-ranked 13^{th} U_ Niño4 (Figure 1). In other words, like the 2023 one, the 2009 El Niño was also accompanied by a weak Southern Oscillation due to the relatively westward extension of SST warming. More importantly, the mixed layer heat budget in the WP with all the three oceanic reanalysis datasets was nearly identical during both the 2009 and 2023 El Niño events, exhibiting weak nonlinear dynamical processes (Figures S19–S21A) that could be further attributed to weak anomalous temperature gradients induced by the high WWV_west accumulated during the preceding multi-year La Niña (Figures S19–S21B–C). Consequently, the mechanism derived from the 2023 event may represent a generalizable pathway for El Niño evolution following prolonged La Niña events, helping to understand the lower-than-expected occurrence of strong El Niño after multi-year La Niñas. It should be noted, however, that a longer duration does not guarantee that a multi-year La Niña will produce a strong enough heat recharge for strong El Niño occurrence, and also western Pacific warm water accumulation for relatively westward SST warming. Therefore, a multi-year La Niña should not be considered a sufficient condition for the mechanism described above, but rather a significant precursor with important indicative value. On the other hand, if a single-year La Niña could indeed produce a subsurface initial state comparable to that following a multi-year event, a similar outcome would be expected. However, in reality, a single-year La Niña rarely reaches an intensity sufficient to induce effects as strong as those of multi-year events.

While prior studies rightly emphasize that lingering central Pacific cold

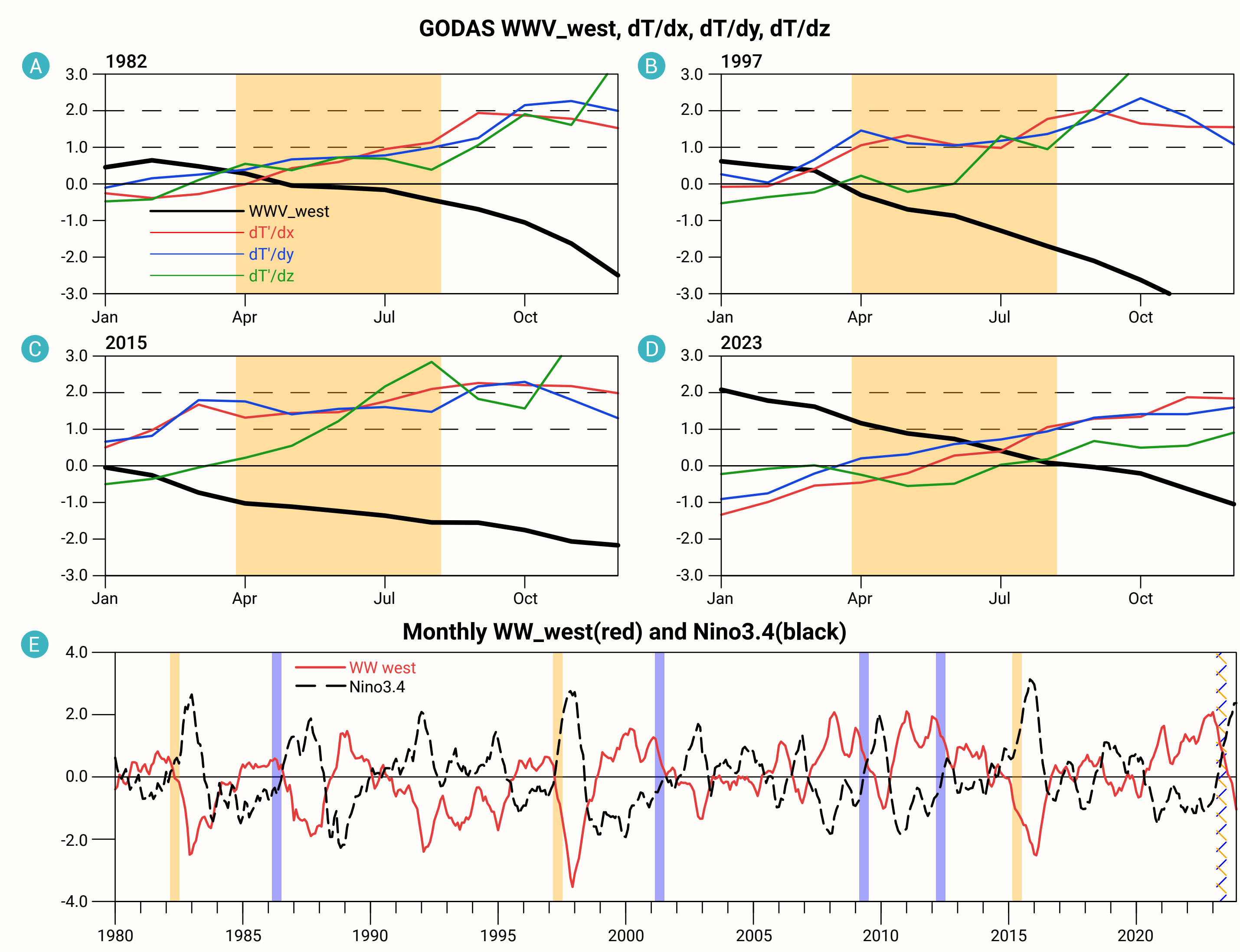

Figure 6. Weak temperature gradient related to high warm water volume in the western Pacific (WWV_west) during 2023 El Niño event (A)–(D) Monthly time-series of the three-dimensional gradients of mixed layer temperature anomalies and WWV_west in the region of 150°E–170°W, 5°S–5°N during the 1982 (A), 1997 (B), 2015 (C), and 2023 (D) El Niño events. The orange shadings denote the periods from March to August. (E) Monthly time series of WWV_west and Niño3.4 from 1980 to 2024. The orange (blue) shadings denote the January-to-August periods in the three extreme El Niño events (after the four multi-year La Niña events that occurred in 1983–1985, 1998–2001, 2007–2008 and 2010–2011). The 2023 El Niño event, succeeding the 2020–2022 multi-year La Niña event, is highlighted by cross-hatching in orange and blue. Note that all the indices have been standardized.

anomalies from multi-year La Niña can suppress westerly anomalies via local air-sea or tropics-subtropics interactions,[11,14,49] these mechanisms fail to fully explain the persistent absence of westerly anomalies after SST anomalies turn positive (e.g., post-May 2023). Our findings resolve this paradox by introducing a tropical Pacific-internal pathway: the accumulated WWV_west from preceding multi-year La Niña weakens anomalous subsurface temperature gradients and nonlinear dynamical cooling in the western Pacific. This, in turn, leads to the westward extension of SST warming and uniform positive convection across the equatorial Pacific, which results in weak Southern Oscillation and westerly anomalies. Thus, the phenomenon of a "strong El Niño but weak Southern Oscillation" following multi-year La Niña appears to be driven by ocean-atmosphere dynamics within the tropical Pacific, a process that is hopefully predictable.

However, this "strong El Niño but weak Southern Oscillation" phenomenon remains challenging to be captured by coupled climate models. We categorized and compared strong El Niño events in the CESM1/2 piControl simulations into two types: those following multi-year La Niña events and those emerging from neutral initial conditions. The results reveal two biases respectively in the ocean and atmospheric models. In ocean models, the cold tongue bias of SST climatology leads to an overly westward extension of SST warming in the both types of El Niño events, which diminishes the contrast in the western boundary of warm SST between the events following multi-year La Niña (Figures 7A & I) and ENSO-neutral state (Figures 7E & M). Since CESM1 and CESM2 share the same ocean component, this feature is similarly manifested in both model versions. The second bias lies in the precipitation response, which aligns with our self-conducted atmospheric experiments forced by observed SST anomalies. Even when driven by observed differentiated SST anomaly patterns, the atmospheric model consistently exhibits an overly pronounced dipole bias in convective response over the western Pacific to the Maritime Continent (Figures 3A–B & D–E). Although CAM6 shows improved precipitation simulation compared to CAM5 due to upgrades in cloud microphysics, the overall performance of the coupled CESM2 experiments shows limited improvement over CESM1 when combined with the ocean model bias (Figure 7). Nevertheless, by demonstrating the underlying physical processes, our findings highlight a potential pathway to improving model simulations and predictions of such atypical ENSO events.

Lastly, it is noteworthy that while the WWV index, functioning as an ENSO precursor that measures ocean heat content (OHC) by integrating the water volume above the 20°C isotherm,[6] effectively captures the wind stress curl-forced basin-wide meridional warm water exchange, i.e. the Recharge Oscillation, this index does not reflect the zonal asymmetry in subsurface warm

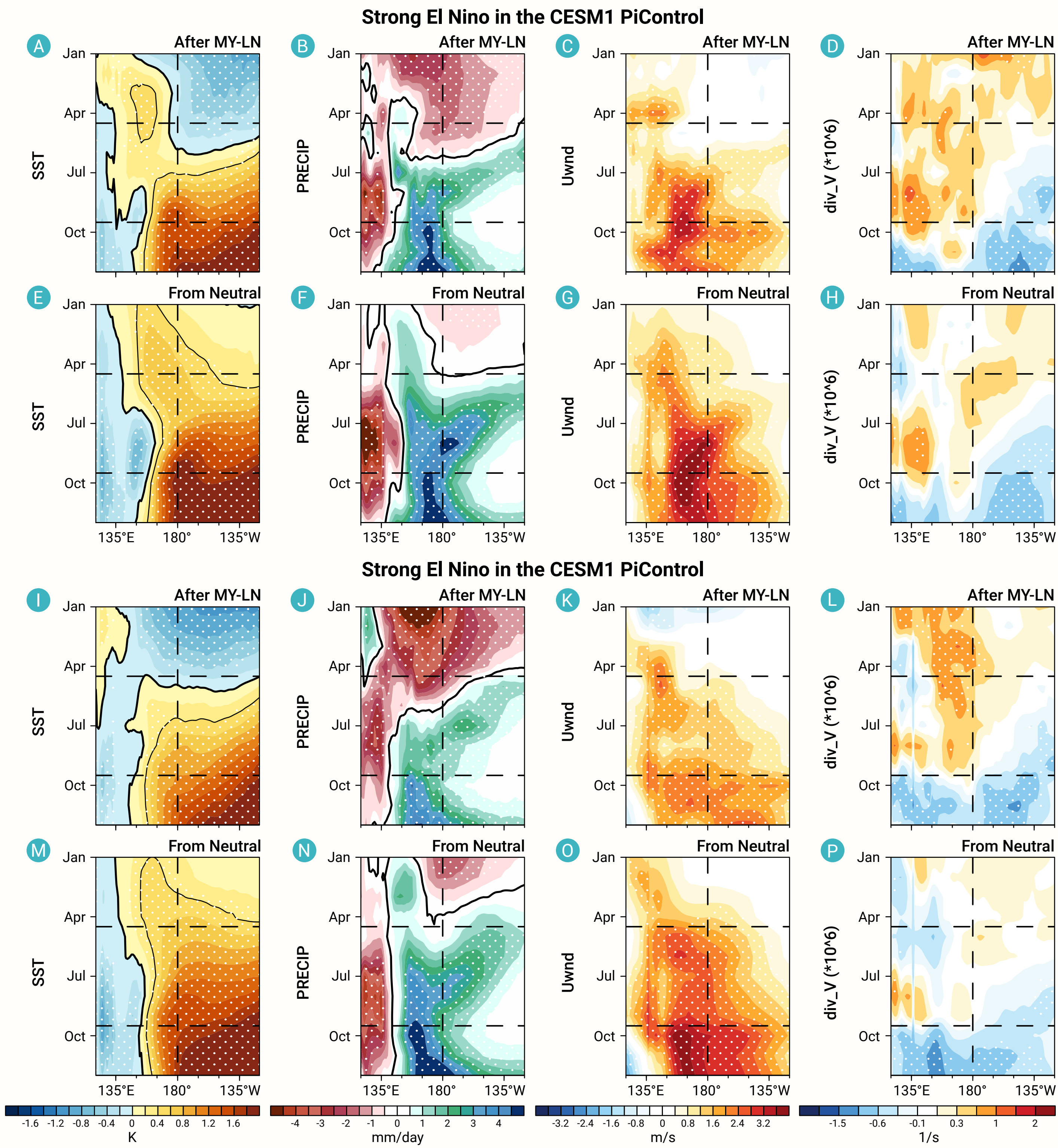

Figure 7. Zonal distribution of ocean-atmosphere variables in the equatorial Pacific during strong El Niño events in the CESM1/2 piControl simulations (A)–(H) Similar to Figure 2, but showing the strong El Niño events following multi-year La Niña (A)–(D) and ENSO-neutral state (E)–(H) in CESM1 piControl simulations. (I)–(P) Similar to (A)–(H), but showing the results in CESM2 piControl simulations. The white dotted region is statistically significant at the 95% confidence level based on the Student's *t*-test.

water or thermocline variations due to its zonal-mean definition. In fact, the zonal asymmetry of OHC has been identified as the "tilt mode",[50] which is highly correlated with the integral of equatorial Pacific-averaged zonal wind stress anomalies over the last 10 months.[51] These two variabilities of OHC can be captured by the first two Empirical Orthogonal Function (EOF) modes of thermocline depth (Figures S22A–B), with their principal components highly correlated with the WWV_west and WWV indices (Figure S22C–D), respectively. While the recharge–discharge mechanism, namely the WWV mode, remains the dominant process governing the cyclic evolution of ENSO, the tilt mode also influences the spatial pattern of SST and the associated atmospheric response, thereby modulating ENSO progression. In extreme cases such as that of 2023, this interaction contributed to an El Niño event that was accompanied by weak Southern Oscillation and westerly wind anomalies. On the other hand, the other three extreme El Niño events were preceded by weak tilt mode conditions (Figures S22C). However, it should be noted that neither the WWV/WWV_west nor the EOF-based indices purely reflect these two physical processes.[52] Moreover, the definition of WWV index encompasses the amount in the western Pacific (i.e., WWV_west index), which, according to our study, is likely to be unfavorable for occurrence of westerly anomalies. Thus, the distribution of subsurface ocean heat content should also be considered to better understand the complexity of ENSO and to supplement the regional mean or EOF-based WWV index for predicting ENSO development.

REFERENCES

1. Timmermann A., An S.-I., Kug J. S., et al. (2018). El Niño–Southern Oscillation complexity. *Nature* **559**:535–545. DOI:10.1038/s41586-018-0252-6
2. Chen D., Lian T., Fu C., et al. (2015). Strong influence of westerly wind bursts on El Niño diversity. *Nat. Geosci.* **8**:339–345. DOI:10.1038/ngeo2399
3. Hasan N. A., Chikamoto Y. and McPhaden M. J. (2022). The influence of tropical basin interactions on the 2020–2022 double-dip La Niña. *Front. Clim.* **4**:1001174. DOI:10.3389/fclim.2022.1001174
4. Li X., Hu Z. Z., McPhaden M. J., et al. (2023). Triple-dip La Niñas in 1998–2001 and 2020–2023: Impact of mean state changes. *J. Geophys. Res. Atmos.* **128**:e2023JD038843. DOI:10.1029/2023JD038843
5. Zhang S., Fan H., Hu X., et al. (2024). Unprecedented cross-equatorial southerly wind anomalies during the 2020–2023 triple-dip La Niña: Impacts and mechanisms. *Atmos. Res.* **304**:107412. DOI:10.1016/j.atmosres.2024.107412
6. Meinen C. S. and McPhaden M. J. (2001). Interannual variability in warm water volume transports in the equatorial Pacific during 1993-99. *J. Phys. Oceanogr.* **31**:1324–1345. DOI:10.1175/1520-0485(2001)031<1324:IVIWWV>2.0.CO;2
7. Lian T., Wang J., Chen D., et al. (2023). A Strong 2023/24 El Niño is staged by tropical Pacific Ocean heat content buildup. *Ocean-Land-Atmos. Res.* **2**:0011. DOI:10.34133/olar.0011
8. Wang J. Z. and Wang C. (2021). Joint boost to super El Niño from the Indian and Atlantic Oceans. *J. Climate* **34**:4937–4954. DOI:10.1175/JCLI-D-20-0710.1
9. Fan H., Wang C., Yang S., et al. (2024). Coupling is key for the tropical Indian and Atlantic oceans to boost super El Niño. *Sci. Adv.* **10**:eadp2281. DOI:10.1126/sciadv.adp2281
10. Hu R., Lian T., Liu T., et al. (2024). Predicting the 2023/24 El Niño from a multi-scale and global perspective. *Commun. Earth Environ.* **5**:675. DOI:10.1038/s43247-024-01867-w
11. Jia F., Cai W., Geng T., et al. (2025). Transition from multi-year La Niña to strong El Niño rare but increased under global warming. *Sci. Bull.* **70**:756–764. DOI:10.1016/j.scib.2024.12.034
12. Hong C. C., Sullivan A. and Chang C. C. (2024). Impact of north Atlantic tripole and extratropical north Pacific extreme SSTs on the 2023/24 El Niño. *Geophys. Res. Lett.* **51**:e2024GL110639. DOI:10.1029/2024GL110639
13. Zhao Y., Li T. and Pan X. (2025). Why zonal wind anomalies were "decoupled" to El Niño in July 2023. *Climate Dyn.* **63**:140. DOI:10.1007/s00382-025-07625-8
14. Kim J., Tian B. and Yu J.-Y. (2025). Unusual and persistent easterlies restrained the 2023/24 El Niño development after a triple-dip La Niña. *npj Clim. Atmos. Sci.* **8**:34. DOI:10.1038/s41612-024-00890-0
15. Lin Y.-F., Chen M., Liu L., et al. (2025). Diverse NPMM conditions deviate the 2023/24 El Niño from the 1997/1998 and 2015/2016 extreme El Niño events. *npj Clim. Atmos. Sci.* **8**:113. DOI:10.1038/s41612-025-01013-z
16. Peng Q., Xie S.-P., Miyamoto A., et al. (2025). Strong 2023–2024 El Niño generated by ocean dynamics. *Nat. Geosci.* **18**:471–478. DOI:10.1038/s41561-025-01700-9
17. Huang B., Thorne P. W., Banzon V. F., et al. (2017). Extended reconstructed Sea surface temperature, Version 5 (ERSSTv5): Upgrades, validations, and intercomparisons. *J. Climate* **30**:8179–8205. DOI:10.1175/JCLI-D-16-0836.1
18. Rayner N. A., Parker D. E., Horton E. B., et al., (2003). Global analyses of sea surface temperature, sea ice, and night marine air temperature since the late nineteenth century. *J. Geophys. Res.: Atmos.* **108**: 4407. DOI: 10.1029/2002JD002670
19. Hirahara S., Ishii M. and Fukuda Y. (2014). Centennial-scale sea surface temperature analysis and its uncertainty. *J. Climate* **27**:57–75. DOI:10.1175/JCLI-D-12-00837.1
20. Schneider D. P., Deser C., Fasullo J., et al. (2013). Climate data guide spurs discovery and understanding. *Eos, Trans. Am. Geophys. Union* **94**:121–122. DOI:10.1002/2013EO130001
21. Xie P. and Arkin P. A. (1997). Global precipitation: A 17-year monthly analysis based on gauge observations, satellite estimates, and numerical model outputs. *Bull. Am. Meteorol. Soc.* **78**:2539–2558. DOI:10.1175/1520-0477(1997)078<2539:GPAYMA>2.0.CO;2
22. Kanamitsu M., Ebisuzaki W., Woollen J., et al. (2002). NCEP–DOE AMIP-II reanalysis (R-2). *Bull. Am. Meteorol. Soc.* **83**:1631–1644. DOI:10.1175/Bams-83-11-1631
23. Hersbach H., Bell B., Berrisford P., et al. (2020). The ERA5 global reanalysis from 1940 to 2022. *Q. J. R. Meteorol. Soc.* **146**:1999–2049. DOI:10.1002/qj.4803
24. Kobayashi S., Ota Y., Harada Y., et al. (2015). The JRA-55 Reanalysis: General specifications and basic characteristics. *J. Meteorol. Soc. of Japan. Ser. II* **93**:5–48. DOI:10.2151/jmsj.2015-001
25. Huang B., Xue Y., Zhang D., et al. (2010). The NCEP GODAS ocean analysis of the tropical pacific mixed layer heat budget on seasonal to interannual time scales. *J. Climate* **23**:4901–4925. DOI:10.1175/2010JCLI3373.1
26. Zuo H., Balmaseda M. A., Tietsche S., et al. (2019). The ECMWF ocean reanalysis system 5 (ORAS5). *Ocean Sci.* **15**:79–808. DOI:10.5194/os-15-779-2019
27. Menemenlis D., Campin J. M., Heimbach P., et al. (2008). ECCO2: High resolution global ocean and sea ice data synthesis. *Mercator Ocean Q. Newsl.* **31**:13–21. https://www.researchgate.net/publication/253471797_ECCO2_High_Resolution_Global_Ocean_and_Sea_Ice_Data_Synthesis
28. Fan H., Huang B., Yang S., et al. (2019). Seasonally-dependent impact of easterly wind bursts on the development of El Niño events. *Climate Dyn.* **53**:1527–1546. DOI:10.1007/s00382-019-04688-2
29. Lin S., Yang S., He S., et al. (2022). Attribution of the seasonality of atmospheric heating changes over the western tropical Pacific with a focus on the spring season. *Climate Dyn.* **58**:2575–2592. DOI:10.1007/s00382-021-06020-3
30. Kay J. E., Deser C., Phillips A., et al. (2015). The community earth system model (CESM) large ensemble project: A community resource for studying climate change in the presence of internal climate variability. *Bull. Am. Meteorol. Soc.* **96**:1333–1349. DOI:10.1175/BAMS-D-13-00255.1
31. Rodgers K. B., Lee S. S., Rosenbloom N., et al. (2021). Ubiquity of human-induced changes in climate variability. *Earth Syst. Dyn.* **12**:1393–1411. DOI:10.5194/esd-12-1393-2021
32. Kim J., Yu J. and Tian B. (2023). Overemphasized role of preceding strong El Niño in generating multi-year La Niña events. *Nat. Commun.* **14**:6790. DOI:10.1038/s41467-023-42373-5
33. Fan H., Wang C. and Yang S. (2023). Asymmetry between positive and negative phases of the Pacific Meridional Mode: A contributor to ENSO transition complexity. *Geophys. Res. Lett.* **50**:e2023GL104000. DOI:10.1029/2023GL104000
34. Amaya D. J., Maher N., Deser C., et al. (2025). Linking projected changes in seasonal climate predictability and ENSO amplitude. *J. Climate* **38**:675–688. DOI:10.1175/JCLI-D-23-0648.1
35. Danabasoglu G., Lamarque J.-F., Bacmeister J., et al. (2020). The community earth system model version 2 (CESM2). *J. Adv. Model. Earth Syst.* **12**:e2019MS001916. DOI:10.1029/2019MS001916
36. Neale R. B., Gettelman A., Park S., et al. (2012). Description of the NCAR Community Atmosphere Model (CAM 5.0). DOI: 10.5065/wgtk-4g06
37. Watanabe M. and Kimoto M. (1999). Tropical - extratropical connection in the Atlantic atmosphere - ocean variability. *Geophys. Res. Lett.* **26**:2247–2250. DOI:10.1029/1999GL900350
38. Jin F. F. (1997). An equatorial ocean recharge paradigm for ENSO. Part I: Conceptual model. *J. Atmos. Sci.* **54**:811–829. DOI:10.1175/1520-0469(1997)054<0811:AEORPF>2.0.CO;2
39. Rasmusson E. M. and Carpenter T. H. (1982). Variations in tropical sea surface temperature and surface wind fields associated with the Southern Oscillation/El Niño. *Mon. Weather Rev.* **110**:354–384. DOI:10.1175/1520-0493(1982)110<0354:VITSST>2.0.CO;2
40. Ropelewski C. F. and Jones P. D. (1987). An extension of the Tahiti–Darwin Southern Oscillation index. *Mon. Weather Rev.* **115**:2161–2165. DOI:10.1175/1520-0493(1987)115<2161:AEOTTS>2.0.CO;2
41. Lindzen R. S. and Nigam S. (1987). On the role of sea surface temperature gradients in forcing low-level winds and convergence in the tropics. *J. Atmos. Sci.* **44**:2418–2436. DOI:10.1175/1520-0469(1987)044<2418:OTROSS>2.0.CO;2
42. Bjerknes J. (1969). Atmospheric teleconnections from the equatorial Pacific. *Mon. Weather Rev.* **97**:163–172. DOI:10.1175/1520-0493(1969)097<0163:ATFTEP>2.3.CO;2
43. Hu Z. Z., McPhaden M. J., Kumar A., et al. (2020). Uncoupled El Niño warming. *Geophys. Res. Lett.* **47**:e2020GL087621. DOI:10.1029/2020GL087621
44. Johnson N. C., L'Heureux M. L., Chang C. H., et al. (2019). On the delayed coupling between ocean and atmosphere in recent weak El Niño episodes. *Geophys. Res. Lett.* **46**:11416–11425. DOI:10.1029/2019GL084021
45. Peng Q., Xie S. P., Passalacqua G. A., et al. (2024). The 2023 extreme coastal El Niño: Atmospheric and air-sea coupling mechanisms. *Sci. Adv.* **10**:sciadv.adk8646. DOI:10.1126/sciadv.adk8646
46. Tan W., Hu Z. Z., McPhaden M. J., et al. (2024). On the divergent evolution of ENSO after the coastal El Niños in 2017 and 2023. *Geophys. Res. Lett.* **51**:2024GL108198. DOI:10.1029/2024GL108198
47. An S.-I. and Jin F.-F. (2001). Collective role of thermocline and zonal advective feedbacks in the ENSO mode. *J. Climate* **14**:3421–3432. DOI:10.1175/1520-0442(2001)014<3421:CROTAZ>2.0.CO;2
48. Kug J. S., Jin F. F. and An S. Il. (2009). Two types of El Niño events: Cold tongue El Niño and warm pool El Niño. *J. Climate* **22**:1499–1515. DOI:10.1175/2008JCLI2624.1
49. Yu J. Y. and Fang S. W. (2018). The distinct contributions of the seasonal footprinting and charged-discharged mechanisms to ENSO complexity. *Geophys. Res. Lett.* **45**:6611–6618. DOI:10.1029/2018GL077664
50. Clarke A. J. (2010). Analytical theory for the quasi-steady and low-frequency equatorial ocean response to wind forcing: The "tilt" and "warm water volume" modes. *J. Phys. Oceanogr.* **40**:121–137. DOI:10.1175/2009JPO4263.1
51. Izumo T., Lengaigne M., Vialard J., et al. (2019). On the physical interpretation of the lead relation between Warm Water Volume and the El Niño Southern Oscillation. *Climate Dyn.* **52**:2923–2942. DOI:10.1007/s00382-018-4313-1

52. Izumo T. and Colin M. (2022). Improving and harmonizing El Niño recharge indices. *Geophys. Res. Lett.* 49:1–10. DOI:10.1029/2022GL101003

FUNDING AND ACKNOWLEDGMENTS

We thank Dr. Qihua Peng for helpful comments during the discussions. This study is supported by the National Natural Science Foundation of China (W2441014, 42192564, 42206026 and 42575025), and the development fund of South China Sea Institute of Oceanology of the Chinese Academy of Sciences (SCSIO202208), the Innovation Group Project of Southern Marine Science and Engineering Guangdong Laboratory (Zhuhai) (316323005) and the Guangdong Province Key Laboratory for Climate Change and Natural Disaster Studies (2023B1212060019). The funders had no role in study design, data collection and analysis, decision to publish, or preparation of the manuscript.

AUTHOR CONTRIBUTIONS

H. F., S. Y. and C. W. conceived the study. H. F. designed and performed the analyses and made the figures. H. F., H. L. and T. W. conducted the model experiments. H. F. and M.X. conducted the ocean heat budget analysis. H. F. wrote the original draft. All authors reviewed and edited the manuscript. All authors contributed to the manuscript and approved the final version.

DECLARATION OF INTERESTS

The authors declare no competing interests.

DATA AND CODE AVAILABILITY

- The ERSSTv5 dataset is from the National Centers for Environmental Information (https://www.ncei.noaa.gov/pub/data/cmb/ersst/v5/netcdf/).
- The HadISST dataset is from the Met Office Hadley Centre (https://www.metoffice.gov.uk/hadobs/hadisst/).
- The COBE SST2 dataset is from the Japan Meteorological Agency (https://ds.data.jma.go.jp/tcc/tcc/products/elnino/cobesst2_doc.html).
- The GPCP dataset is from the NOAA Physical Sciences Laboratory (https://psl.noaa.gov/data/gridded/data.gpcp.html).
- The CMAP dataset is from the NOAA Climate Prediction Center (ftp://ftp.cpc.ncep.noaa.gov/precip/cmap).
- The NCEP2 dataset is from the the NOAA Climate Prediction Center (https://www.cpc.ncep.noaa.gov/products/wesley/reanalysis2/).
- The ERA5 dataset is from the European Centre for Medium-Range Weather Forecasts (https://cds.climate.copernicus.eu/datasets/reanalysis-era5-single-levels?tab=download).
- The JRA55 dataset is from the Japan Meteorological Agency (https://jra.kishou.go.jp/JRA-55/index_en.html).
- The GODAS dataset is from the NOAA Climate Prediction Center (https://ftp.cpc.ncep.noaa.gov/godas/monthly/).
- The ORAS5 dataset is from the European Centre for Medium-Range Weather Forecasts (https://cds.climate.copernicus.eu/datasets/reanalysis-oras5?tab=download).
- The ECCO2 dataset is from the NASA Jet Propulsion Laboratory (https://cds.climate.copernicus.eu/datasets/reanalysis-oras5?tab=download).
- The WWV index is downloaded from https://www.pmel.noaa.gov/tao/wwv/data/.

SUPPLEMENTAL INFORMATION

It can be found online at https://doi.org/10.59717/j.xinn-geo.2026.100224.